

Fluctuations in Northern Hemisphere 700 mb Height Field Associated with the Southern Oscillation

W. Y. CHEN

Climate Analysis Center, NMC, NWS, NOAA Washington, DC 20746

(Manuscript received 6 November 1981, in final form 16 March 1982)

ABSTRACT

Variations in the mid-troposphere circulation associated with the Southern Oscillation (SO) are investigated and documented using mean monthly 700 mb height data for the period 1951-79. The SO was defined by a Southern Oscillation Index (SOI) consisting of the difference in normalized mean monthly sea-level pressures at Tahiti and Darwin. Results for all four seasons are presented in the form of lagged, as well as contemporaneous, correlations and composites of height anomalies obtained separately for high and low SOI values.

Different SO teleconnection patterns are observed for each season. Strongest SO signals appear in the winter with SOI leading the height field by one to two seasons. The time lead may be useful in prognostic applications. The correlation in the summer is negligible. The winter teleconnection pattern over the North Pacific-North America-North Atlantic sector is similar to that shown by Bjerknes and others. Patterns for other seasons are also presented. The statistical significance of the various teleconnections patterns is discussed.

Distinct features are observed for the high and low SOI composites, where low SOI's are closely related to above normal equatorial central Pacific sea-surface temperatures. The high SOI composite in winter shows a tendency for more pronounced North America negative anomalies and North Atlantic positive anomalies, suggesting an association with one of the two phases of the North Atlantic Oscillation. The high SOI composites of other seasons also show more pronounced anomalies in various regions.

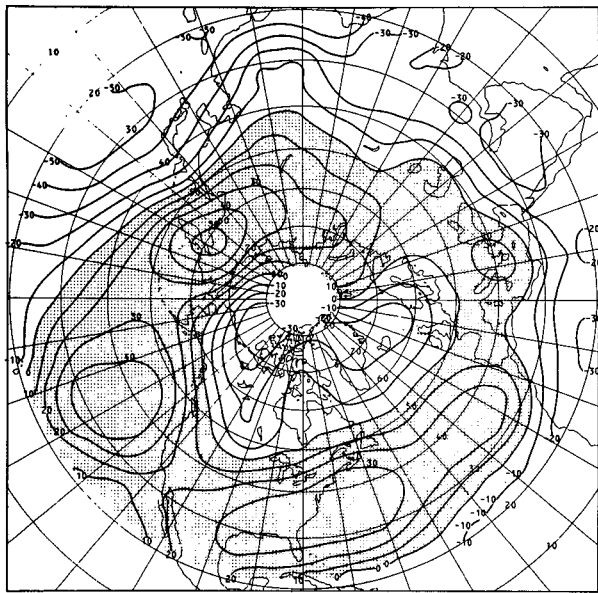
1. Introduction

The Southern Oscillation (SO) and its associated short-term climatic variations has received increasing attention in recent years. As described by Walker and Bliss (1932, 1937), Berlage (1957, 1966) and Troup (1965), the SO is an irregular, interannual and global-scale fluctuation reflecting a shift of mass between the Indonesian equatorial low pressure cell and South Pacific subtropical anticyclone. Intimately related to the SO are the equatorial zonal east-west Walker Circulation (Bjerknes, 1969), El Niño, an occasional warming of sea-surface temperature off the west coast of South America (Wyrtki, 1973, 1975; Quinn, 1974), and several coherent pulses of meteorological and oceanographic variables, such as rainfall, sea-surface temperatures, air temperature, winds and sea level, in the tropical Pacific belt (Troup, 1965; Krueger and Winston, 1974; Kidson, 1975; Trenberth, 1976; Wright, 1979). A recent review of the Southern Oscillation can be found in Julian and Chervin (1978) and Rasmusson and Carpenter (1982).

A link of SO to the midlatitude systems and long waves in the westerlies has also been observed by Walker and Bliss (1932, 1937), Bjerknes (1966, 1969), Trenberth (1976), Namias (1976), Wright

(1977, 1978), and most recently, by Trenberth and Paolino (1981), van Loon and Rogers (1981) and van Loon and Madden (1981). The physical processes responsible for the link were postulated by Bjerknes as a weakening of the easterlies over the equatorial Pacific leading to cessation of equatorial upwelling and, thus, above normal sea-surface temperature which results in an enhanced Hadley circulation and above-average poleward transport of angular momentum to the midlatitude belt of the westerly winds in the Pacific sector. The downwind effects of the North Pacific circulation may explain the teleconnection patterns over North America and the North Atlantic. Most recently, however, Horel and Wallace (1981) present a three-dimensional dynamical interpretation of the links based on the results of the numerical models of Opsteegh and Van den Dool (1980), Hoskins and Karoly (1981) and Webster (1981). The theoretical studies demonstrate a response to tropical forcing of wave trains as well as vertical structures that bear qualitative resemblances to the SO teleconnection patterns observed by Horel and Wallace in the Northern Hemisphere during the winter.

Since this is mainly an observational analysis, the present article focuses on a documentation of the variations in the Northern Hemisphere mid-tropo-



CORRELATION BETWEEN DJF SOI & DJF 700 MB HEIGHT

FIG. 1. Contemporaneous cross-correlations between SOI's and 700 mb heights for the winter season for the period 1950/51 to 1978/79. The shaded areas are positive and the contour interval is 0.1.

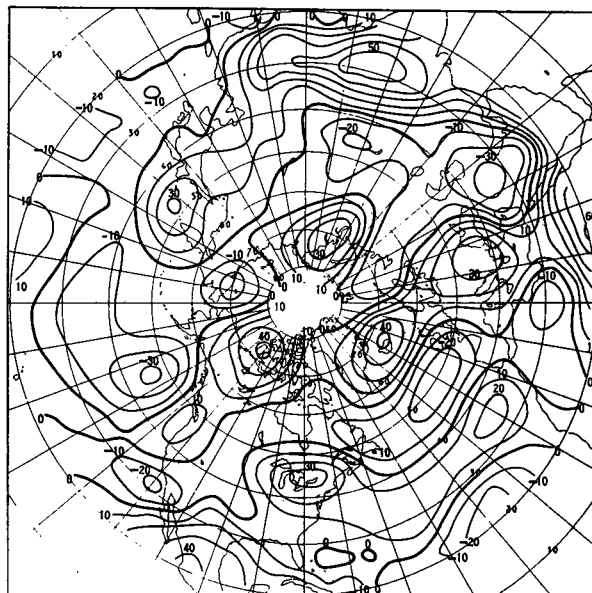


FIG. 2. One-year lagged autocorrelation coefficients of the winter 700 mb heights for the period 1950/51 to 1978/79. The contour interval is 0.1.

sphere circulation associated with the SO. Series of lagged as well as contemporaneous cross-correlations between the Southern Oscillation Index (SOI) and 700 mb heights were obtained for all four seasons. Composites of height anomalies were also con-

structed separately for large positive and negative departures of SOI to discern the contribution to the teleconnection patterns associated with each case. The results for each season are presented in the following sections after a brief description of the data used.

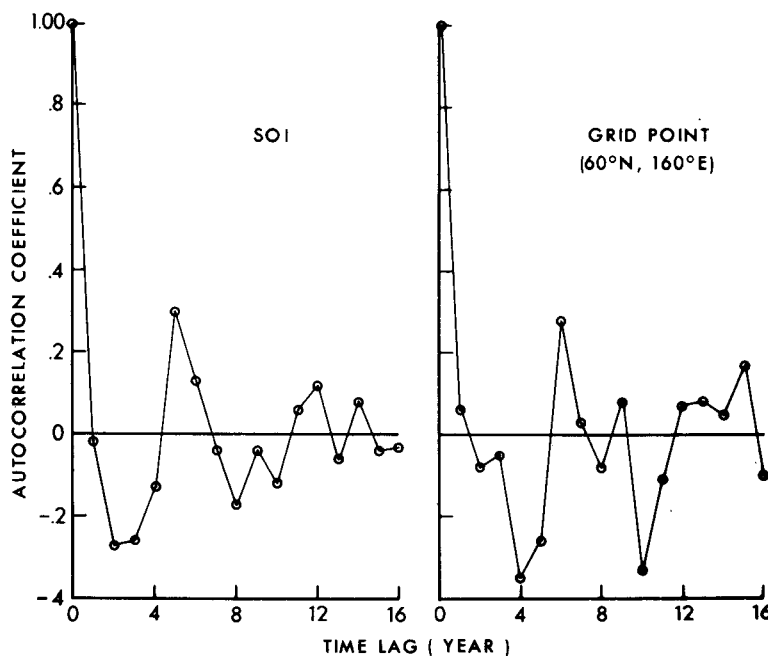


FIG. 3. Autocorrelation coefficients of winter SOI's and the winter time series of 700 mb height field at 60°N and 160°E.

TABLE 1. Tabulated integral time scale τ (years) up to the i th term of Eq. (3) and the final τ , effective number of degrees of freedom n , and correlation value of 5% probability level $C_{0.975}$.

i of Eq. (3)	Location of grid point				
	25°N 150°E	60°N 160°E	75°N 130°W	35°N 75°W	35°N 140°W
0	1.00	1.00	1.00	1.00	1.00
1	1.00	1.00	0.98	0.99	1.00
2	1.06	1.04	0.92	0.98	1.10
3	1.13	1.07	1.00	1.00	1.14
4	1.22	1.16	1.06	1.07	1.15
5	1.29	1.01	0.83	1.04	1.22
6	1.39	1.08	0.75	1.03	1.10
7	1.39	1.08	0.76	1.04	1.11
8	1.43	1.10	0.76	1.00	1.10
9	1.42	1.10	0.75	1.00	1.09
10	1.49	1.18	0.71	1.01	1.05
11	1.50	1.16	0.73	1.00	1.05
12	1.54	1.18	0.70	0.97	1.10
13	1.55	1.17	0.73	0.97	1.12
14	1.55	1.18	0.69	0.98	1.11
15	1.55	1.16	0.70	0.97	1.10
16	1.55	1.17	0.70	0.98	1.11
τ	1.55	1.17	1.00	1.00	1.11
n	19	25	29	29	26
$C_{0.975}$	0.44	0.40	0.36	0.36	0.39

2. Data description

Mean monthly 700 mb height data, in $5^\circ \times 5^\circ$ latitude-longitude grids, north of 20°N , for the period 1951–79, were used in this analysis. The data are maintained by the Prediction Branch, Climate Analysis Center, National Meteorological Center, NOAA. The SO was defined by the SOI's consisting of the difference in normalized mean monthly sea-level pressures at Tahiti (17°S , 150°W) and Darwin (12°S , 131°E). The advantage of choosing this index among other sea-level pressure indices is discussed by Chen (1982).

Since the low-frequency interannual fluctuations are the quantities of interest here, the prominent annual variations of the data were first removed by subtracting the 29-year average monthly values from the individual months. This was done for both 700 mb heights and SOI data. The seasonal means were then obtained by averaging the three adjacent monthly anomalies centered in January, April, July and October, respectively. For the winter season of 1951, data of December 1950 were also used. The 29 anomalies of each season were then used in this analysis. None of the time series used were filtered or detrended.

3. Winter teleconnections and composites

The winter 700 mb height anomalies at each grid point are cross correlated with SOI of various seasons

to reveal the SO signatures in the winter height field. The potentially useful information of time lead/lag relationship between the two parameters is investigated in this section. Also studied are the composites of anomalies obtained separately for the high and low SOI values.

a. Contemporaneous correlations

The contemporaneous cross-correlation coefficient is defined as

$$C_{xy} = \frac{1}{N} \sum_{i=1}^N [X(i\Delta t) - \bar{X}][Y(i\Delta t) - \bar{Y}] / N S_x S_y, \quad (1)$$

where $X(t)$ and $Y(t)$ are the input time series sampled with time interval Δt . The total length of time is $T = N\Delta t$. The overbar denotes means, while S_x and S_y are the standard deviations of $X(t)$ and $Y(t)$, respectively.

The winter coefficients were obtained according to Eq. (1) for the period 1950/51 to 1978/79. Note that $\Delta t = 1$ year and $N = 29$. The results are presented in Fig. 1, where a large-scale pattern emerges with certain regions having positive associations with the SOI while others are negatively correlated.

The correlation coefficients exceed 0.5 in some areas. However, the significance of these values, as well as the pattern, needs to be established. For this purpose the autoregressive natures of the two parameters were investigated first. The one-year lag autocorrelation of SOI is -0.02 and those of the height field at each grid point are presented in Fig. 2. Al-

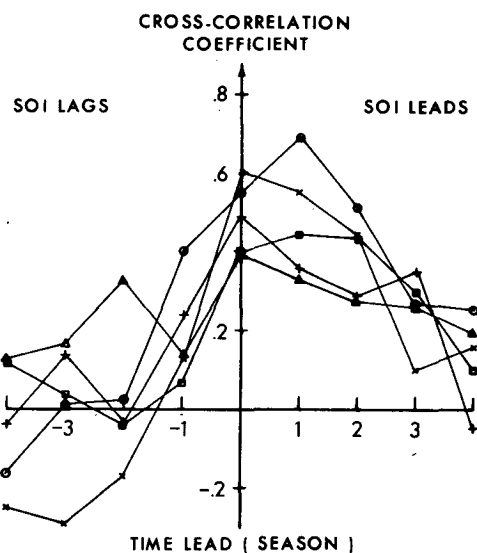


FIG. 4. Cross-correlation coefficients between SOI's and height fields at 25°N , 150°E (\times); 60°N , 160°E (\circ); 75°N , 130°W (Δ); 35°N , 75°W (\square); and 35°N , 140°W ($+$). Inversed values are plotted for those in symbols (\times) and (Δ).

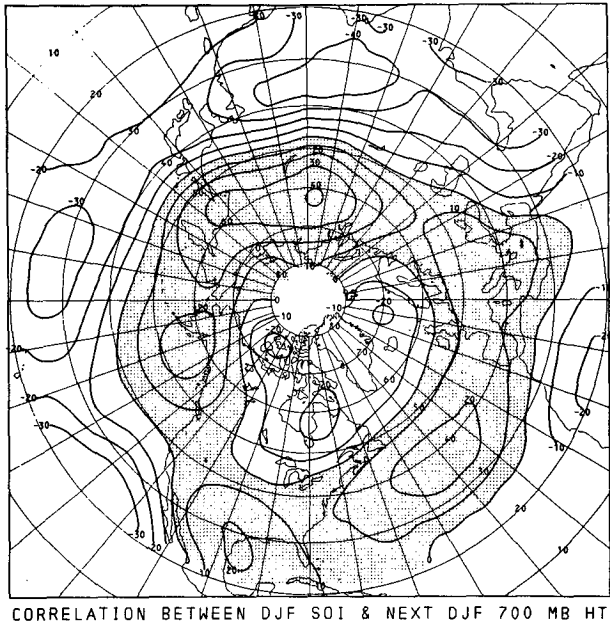
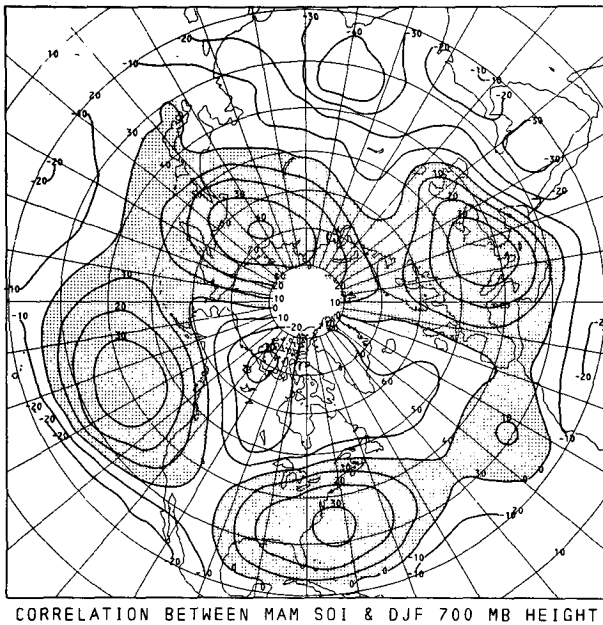
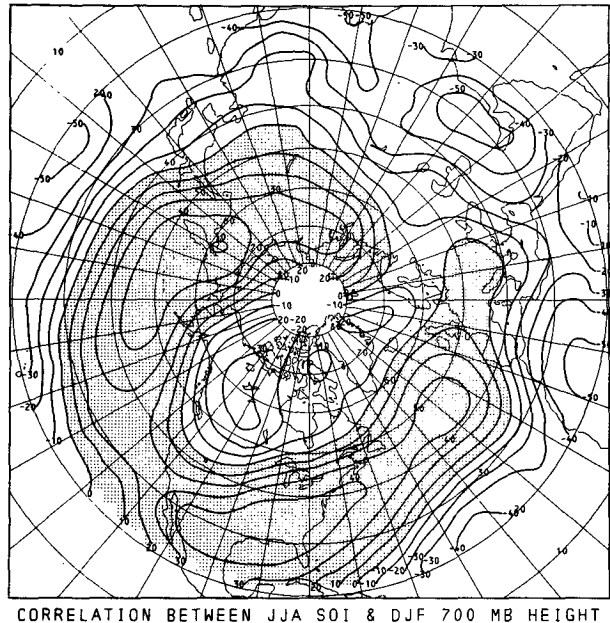
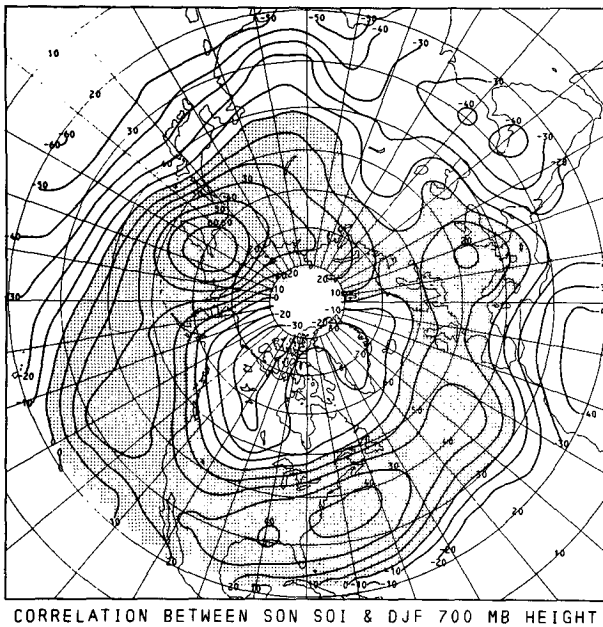


FIG. 5. Lagged cross-correlation coefficients between winter height fields and SOI's of various preceding seasons. The shaded areas are positive and the contour interval is 0.1.

though the SO is well known to exhibit high season-to-season persistence, it is seen that the present winter-to-winter autocorrelation is quite small. The 700 mb height one-year lag autocorrelations are, for most parts, no greater than that of the SOI. In those regions where they show large cross-correlations (Fig. 1), the winter-to-winter persistence is easily seen (Fig. 2) to be low. Thus it can be preliminarily judged that the large-scale pattern of Fig. 1 may be mean-

ingful. The value beyond which a cross-correlation becomes statistically significant remains to be determined.

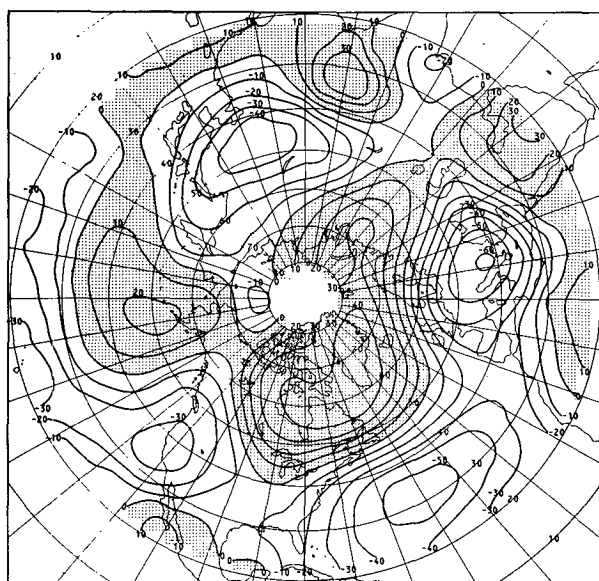
Since the effective number of degrees of freedom (EDOF) may not be the same as the number of data that enter into the calculation of the results of Fig. 1, a special effort was made to obtain the EDOF for those regions that show large cross-correlation values. The relationship between the autoregressive na-

TABLE 2. Integral time scale τ (years). Effective number of degrees of freedom n , and correlation value of 5% probability level $C_{0.975}$ at a few representative locations for various seasons.

Correlations	Grid point	τ	n	$C_{0.975}$
JJA SOI to	20°N, 160°E	1.18	25	0.40
DJF height	60°N, 160°E	1.17	25	0.40
fields	60°N, 120°W	1.00	29	0.36
	35°N, 90°W	1.00	29	0.36
	25°N, 5°W	1.16	25	0.40
	30°N, 60°E	1.06	27	0.38
JJA SOI to	45°N, 180°W	1.00	29	0.36
SON height	65°N, 75°W	1.12	26	0.39
fields	40°N, 15°W	1.03	28	0.37
	80°N, 100°E	1.09	27	0.38
	20°N, 75°E	1.00	29	0.36
JJA SOI to	50°N, 125°E	1.07	27	0.38
JJA height	60°N, 140°W	1.00	29	0.36
fields	60°N, 75°W	1.07	27	0.38
	35°N, 0°E	1.02	28	0.37
	70°N, 65°E	1.00	29	0.36
MAM SOI to	35°N, 145°E	1.00	29	0.36
MAM height	50°N, 80°W	1.23	24	0.40
fields	75°N, 95°W	1.02	28	0.37
	35°N, 40°W	1.14	25	0.40
	35°N, 5°W	1.21	24	0.40

ture and the EDOF is discussed in some detail by Davis (1976). He presents a method of estimating n , the EDOF, as

$$n = \frac{N\Delta t}{\tau}, \quad (2)$$



CORRELATION BETWEEN NOISE AND DJF 700 MB HEIGHT

FIG. 6. Cross-correlation coefficients between random data and 700 mb winter height anomalies. An example shows high correlations due to chance occurrence. The shaded areas are positive and the contour interval is 0.1.

TABLE 3. Percentage of area (POA) that the cross-correlations of SOI and height field exceed the corresponding critical values determined by Davis' formula.

SOI leads height field by (season)	DJF	POA MAM	JJA	SON
0	11.44	11.92	4.62	10.01
1	17.19	9.55	4.65	8.77
2	21.49	7.25	1.46	1.35

where

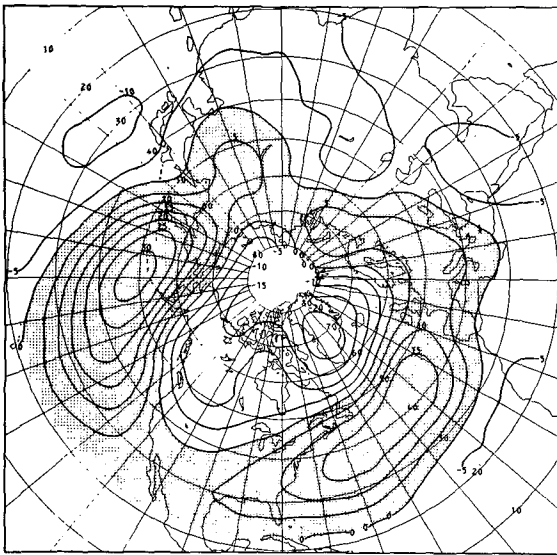
$$\tau = \sum_{i=-\infty}^{\infty} C_{xx}(i\Delta t)C_{yy}(i\Delta t)\Delta t, \quad (3)$$

and C_{xx} and C_{yy} are the discrete autocorrelation coefficients of $X(t)$ and $Y(t)$, respectively. The integral time scale τ determines the time period required to gain a new degree of freedom in the estimation of the cross-correlation.

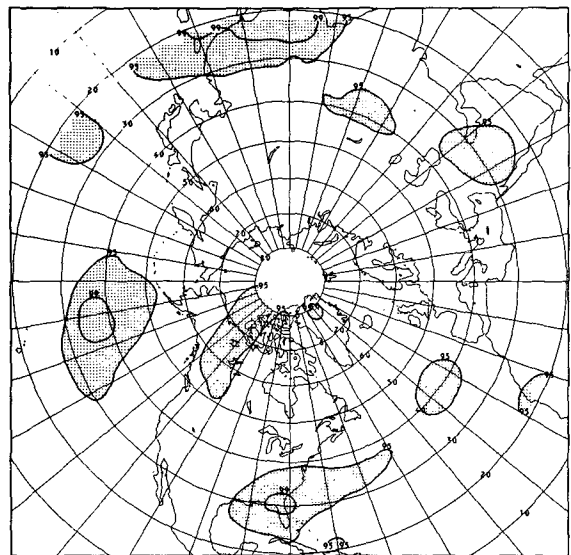
Applying Davis' method, τ and n at various grid points were evaluated. The time series at grid point (60°N, 160°E), which has one of the highest correlation values, is chosen as an illustration. Its autocorrelation function as well as that of the SOI are

TABLE 4. Three categories of Southern Oscillation anomaly. The high, medium and low value are denoted by H, M and L, respectively. The winter index consists of January and February of the year listed and December of the previous year.

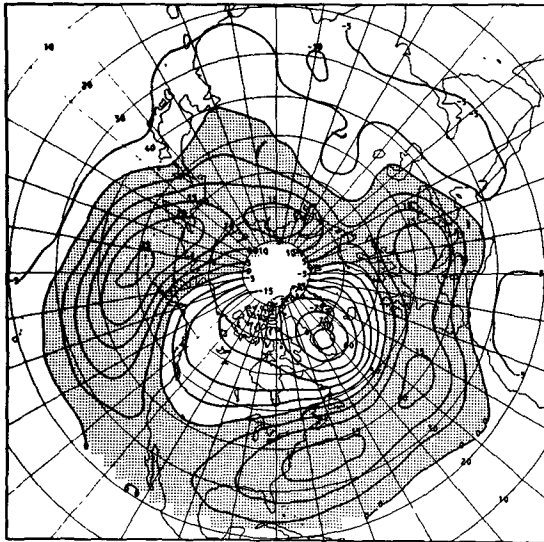
Year	Winter DJF	Spring MAM	Summer JJA	Autumn SON
1950	H	H	H	H
1	H	L	L	L
2	L	M	M	M
3	L	L	L	L
4	M	M	M	M
5	M	H	H	H
6	H	H	H	H
7	M	M	L	L
8	L	L	M	M
9	L	M	M	M
1960	M	M	M	H
1	M	M	M	M
2	H	M	M	M
3	M	M	L	L
4	L	H	H	H
5	M	L	L	L
6	L	L	M	M
7	H	M	M	M
8	M	M	H	M
9	L	L	L	L
1970	L	M	M	H
1	H	H	H	H
2	M	L	L	L
3	L	M	H	H
4	H	H	H	H
5	M	H	H	H
6	H	H	L	L
7	M	L	L	L
8	L	M	M	M
9	M	M	M	L



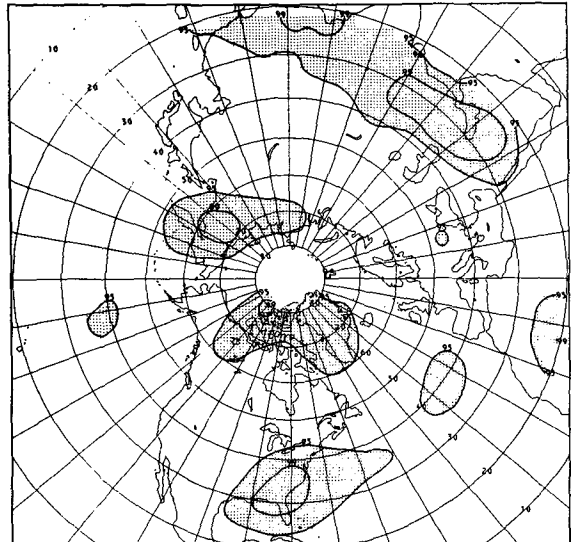
DJF 700 MB ANOMALIES FOR HGH SOI YEARS, LAG=0



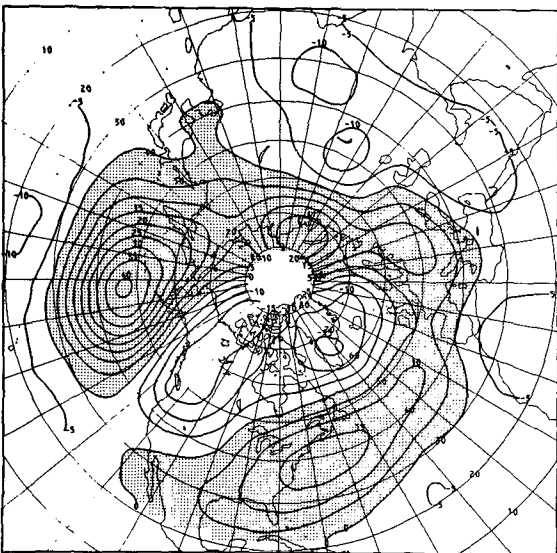
CONF.LIMIT OF DJF COMPOSITE FOR HGH SOI YRS,LAG=0



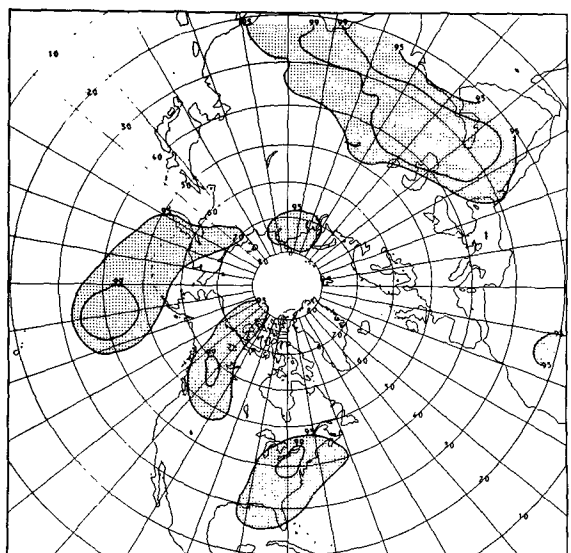
DJF 700 MB ANOMALIES FOR HGH SOI YEARS, LAG=1



CONF.LIMIT OF DJF COMPOSITE FOR HGH SOI YRS,LAG=1

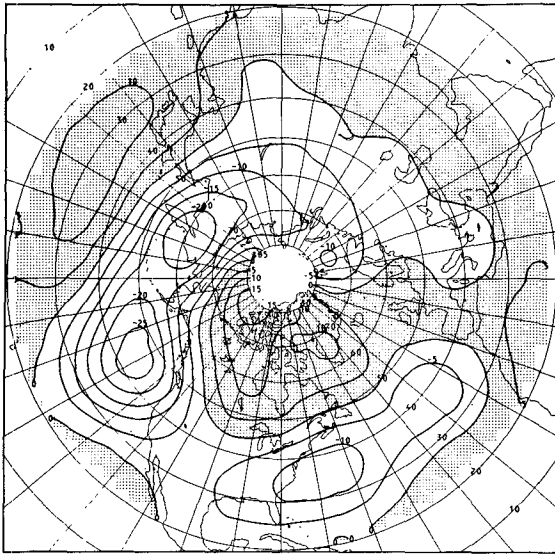


DJF 700 MB ANOMALIES FOR HGH SOI YEARS, LAG=2

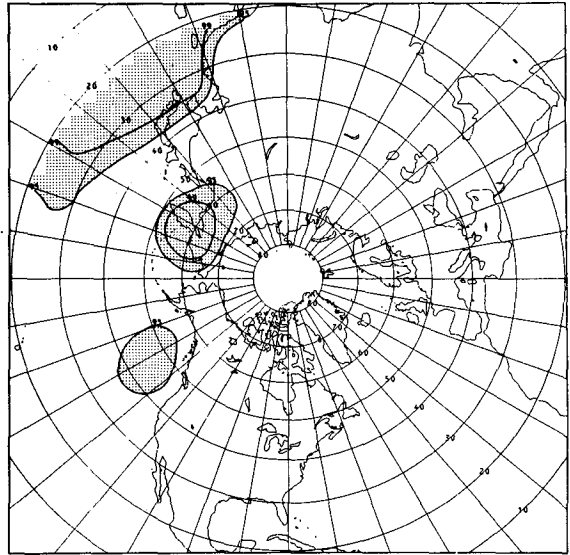


CONF.LIMIT OF DJF COMPOSITE FOR HGH SOI YRS,LAG=2

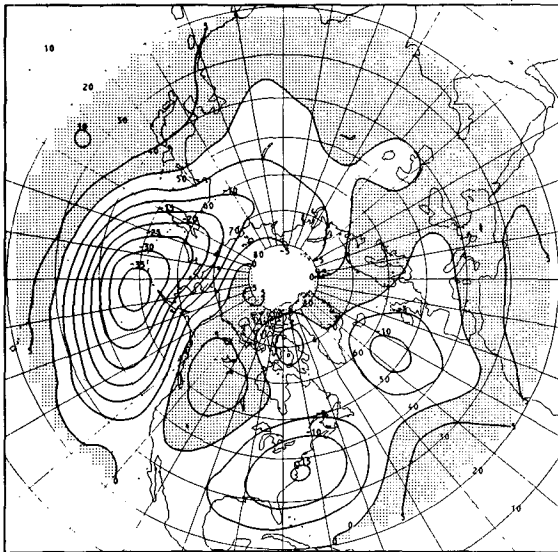
FIG. 7. Winter composites associated with high SOI values with the latter leading the height field by various seasons. The shaded areas are positive and the contour interval is 5 m. Confidence limits of the anomalies are presented on the right.



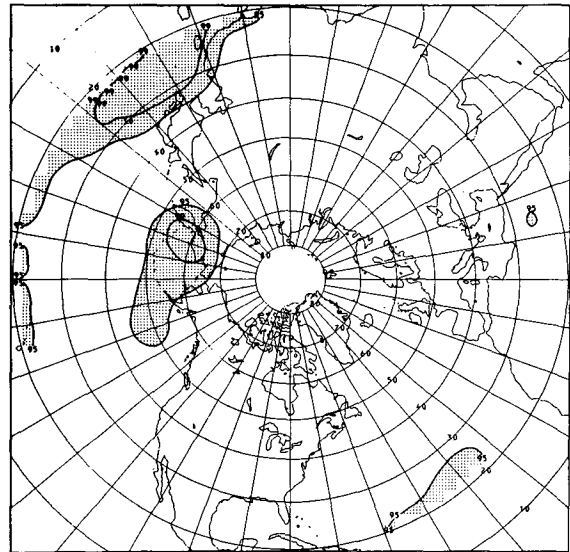
DJF 700 MB ANOMALIES FOR LOW SOI YEARS, LAG=0



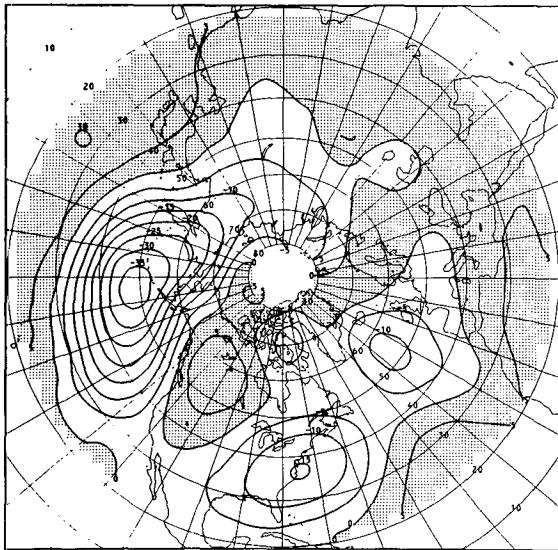
CONF.LIMIT OF DJF COMPOSITE FOR LOW SOI YRS, LAG=0



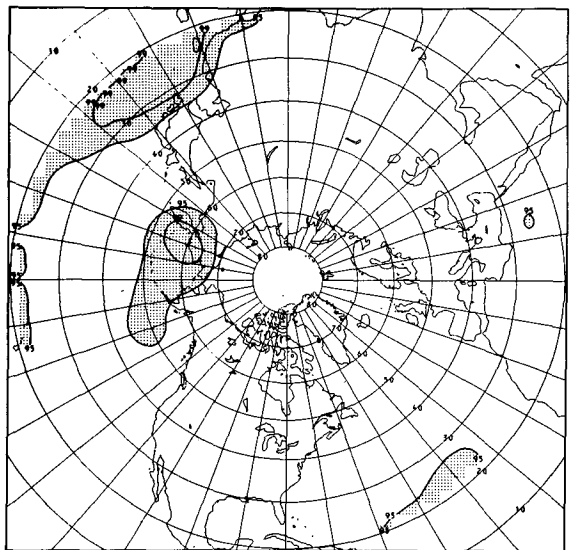
DJF 700 MB ANOMALIES FOR LOW SOI YEARS, LAG=1



CONF.LIMIT OF DJF COMPOSITE FOR LOW SOI YRS, LAG=1



DJF 700 MB ANOMALIES FOR LOW SOI YEARS, LAG=2



CONF.LIMIT OF DJF COMPOSITE FOR LOW SOI YRS, LAG=2

FIG. 8. As in Fig. 7, associated with low-SOI values.

shown in Fig. 3. Eq. (3) is used to obtain τ for various number of i , and the results are listed in Table 1. Also presented are those of four other grid points which represent, respectively, the four other centers of higher correlations in the Northern Hemisphere. The integral time scale ranges from less than 1 to ~ 1.55 years. The EDOF can thus be obtained through Eq. (2) and the critical cross-correlation value for various significance levels can be found readily from the standard tables (e.g., Dixon and Massey, 1957). At the bottom of Table 1, the cross-correlation values at 5% significance level are listed for the five grid points. They range from 0.36 to 0.44.

b. Lead/lag relationships

The lead/lag relationship between SOI and the height field is explored first by analyzing the situations at those five grid points mentioned in the previous section. The contemporaneous cross-correlation coefficient of Eq. (1) is extended to allow a time lead by one of the parameters, i.e.,

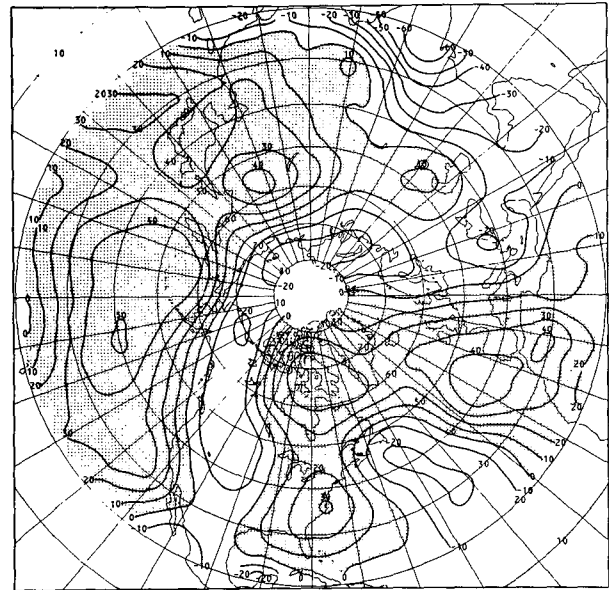
$$C_{xy}(j\Delta s) = \sum_{i=1}^N [X(i\Delta t - j\Delta s) - \bar{X}] \times [Y(i\Delta t) - \bar{Y}] / NS_x S_y, \quad (4)$$

where Δs is another time interval (a season here) and j can be a positive or negative integer. For example, when $j = 2$, X leads Y by two seasons, while $j = -2$ implies X lags Y by two seasons.

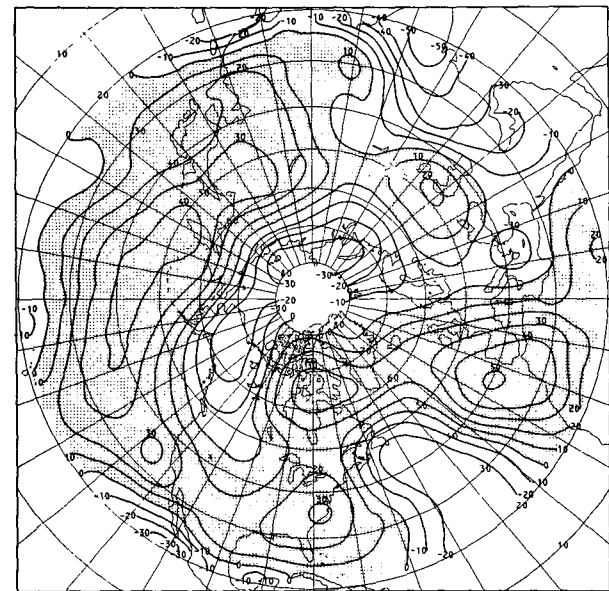
The results of the five lagged cross-correlation functions are shown in Fig. 4, where those of grid points (25°N, 150°E) and (75°N, 130°W) are plotted in inversed values. Note that when SOI lags the height field, the correlation values drop rapidly while the values remain as high or even higher than the zero lag values when the SOI leads by one to two seasons.

Based on the information found above, the entire Northern Hemisphere 700 mb height field north of 20°N was cross correlated with the SOI, with the latter leading the height field by one to four seasons, respectively. The results are shown in Fig. 5. A well-defined teleconnection pattern is observed. The strongest SO signals are found as expected when the SOI leads the height field by a season or two, a characteristic that may be useful in prognostic applications.

The teleconnection pattern over the sector of North Pacific–western Canada–eastern United States is similar to that shown by Bjerknes (1972), Namias (1976) and Horel and Wallace (1981). The pattern also resembles the one obtained by Wright (1977, 1978), who correlates an SOI derived from empirical orthogonal functions with the surface temperature anomalies at many Northern Hemisphere stations. The wintertime climate variations associated with this teleconnection pattern have been discussed in detail by Horel and Wallace (1981).



CORRELATION BETWEEN SON SOI & SON 700 MB HEIGHT



CORRELATION BETWEEN JJA SOI & SON 700 MB HEIGHT

FIG. 9. SOI-associated teleconnections for the autumn season. Temporal lead by SOI's are indicated. The shaded areas are positive and the contour interval is 0.1.

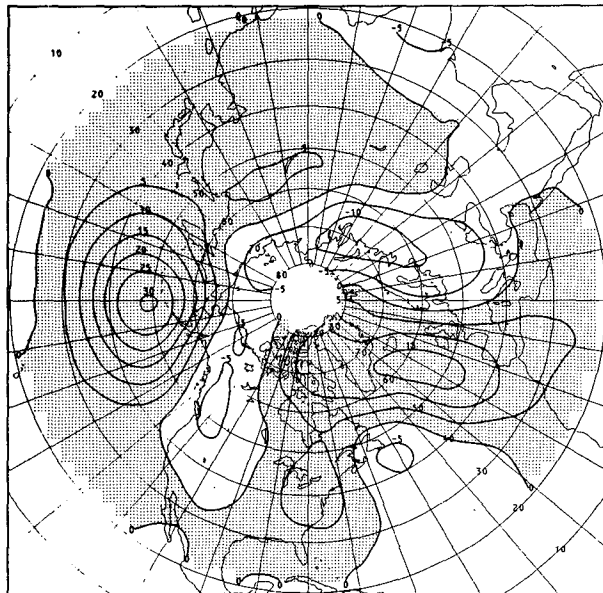
One other interesting feature of Fig. 5, when the SOI precedes the height field a season or two, is the tendency for a more significant negative correlation with the SOI for the Eastern Hemisphere along and south of 30°N.

Since different seasonal SOI's were cross-correlated with the winter 700 mb height field in Fig. 5, and, in addition, there are new centers of large correlation values and slight change in location of the old centers, it should be useful to obtain the values

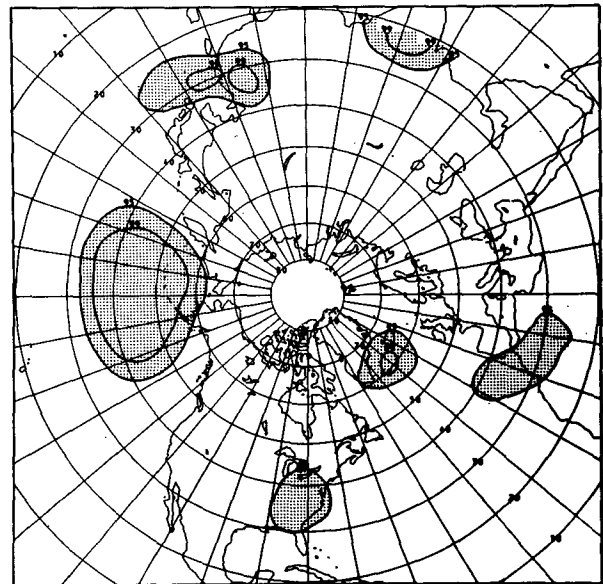
beyond which the correlations are not negligible at a 5% significance level for the regions represented by the centers. Table 2 lists the τ , n and $C_{0.975}$ for the six centers that appear on the teleconnection map when SOI leads the winter height field by two seasons. The $C_{0.975}$ values range from 0.36 to 0.40. If we assume that each center is fairly representative of its neighborhood, then, except for western Canada, a large area surrounding each center is seen to have cross-correlation value higher than the responsive $C_{0.975}$.

c. Statistical significance of patterns

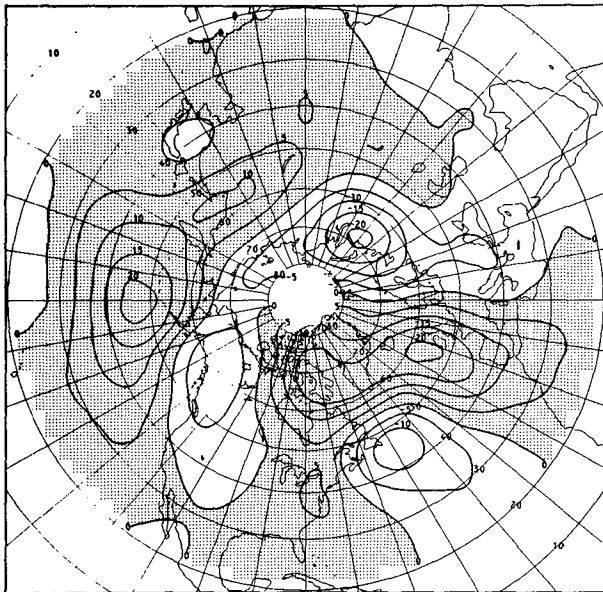
Although the values at which the temporal cross-correlations become statistically significant have been established, the significance of a spatial pattern has yet to be assured. To illustrate the concern, we correlate the winter 700 mb height field with a series of random data, instead of the SOI. The results, shown in Fig. 6, also yield some regions of high positive and negative correlations. However, we are certain that these are entirely owing to chance occur-



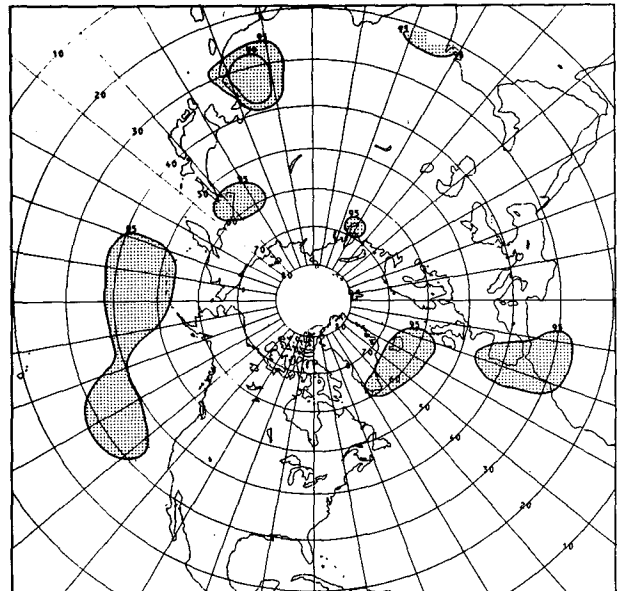
SON 700 MB ANOMALIES FOR HGH SOI YEARS, LAG=0



CONF. LIMIT OF SON COMPOSITE FOR HGH SOI YRS, LAG=0



SON 700 MB ANOMALIES FOR HGH SOI YEARS, LAG=1



CONF. LIMIT OF SON COMPOSITE FOR HGH SOI YRS, LAG=1

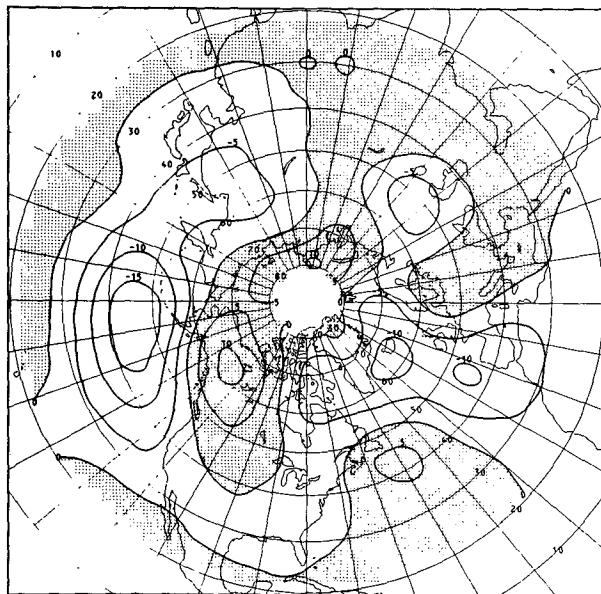
FIG. 10. Autumn composites and confidence limits associated with high-SOI values. On the composites, the shaded areas are positive and the contour interval is 5 m.

rence. The question then is how significant are the SO teleconnection patterns of Fig. 1? How much confidence does one have that these patterns are not due to chance occurrence?

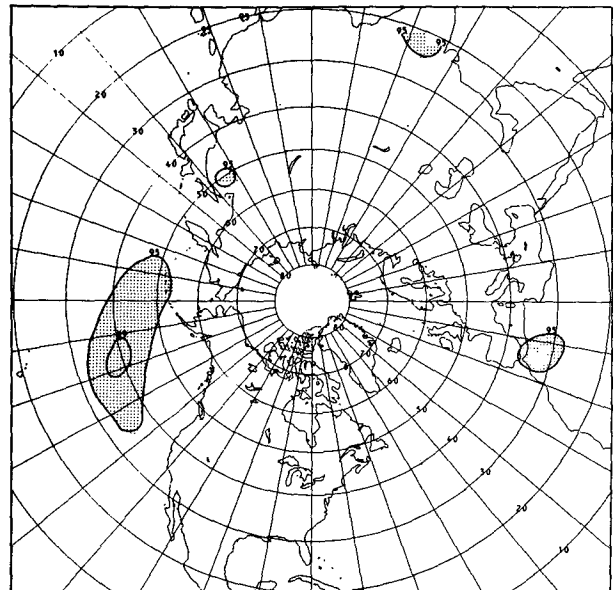
Viewing the growing interest in the SO and its influence on other parts of the globe, Livezey and Chen conducted a critical analysis on the subject mentioned above. The result will be published in a separate paper. It is sufficient here to say that a Monte Carlo approach was employed to correlate the height field with random data, and the percentage of area (POA) that the correlations exceed the crit-

ical value, which is 0.367 for 29 temporal degrees of freedom at the 5% significance level, was determined. The experiments were conducted 200 times, each with different random data. From the frequency distribution of the 200 POA's, the 95 and 99% confidence limits can be determined; these turn out to be 12.93 and 18.09%, respectively.

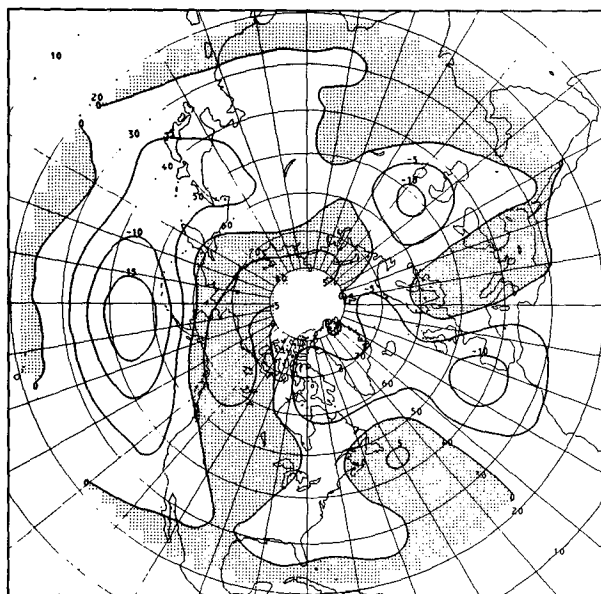
The corresponding POA's of the SOI teleconnection patterns were obtained by counting those exceeding the critical correlation values determined by the Davis' method mentioned in Section 3a. The values thus obtained are listed in Table 3. Note that the



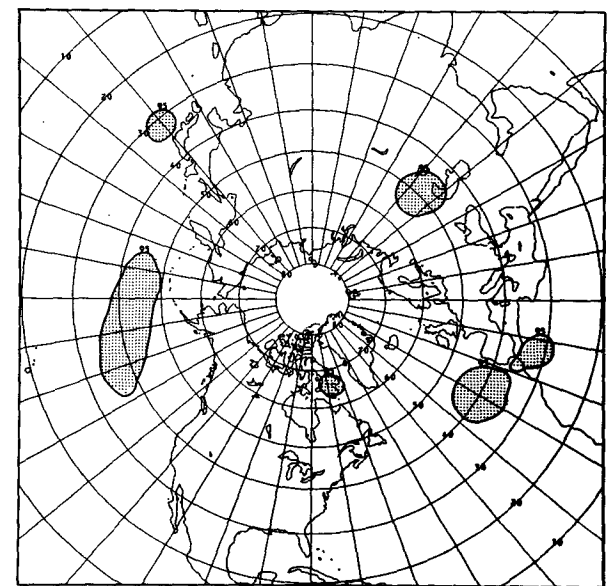
SON 700 MB ANOMALIES FOR LOW SOI YEARS, LAG=0



CONF. LIMIT OF SON COMPOSITE FOR LOW SOI YRS, LAG=0

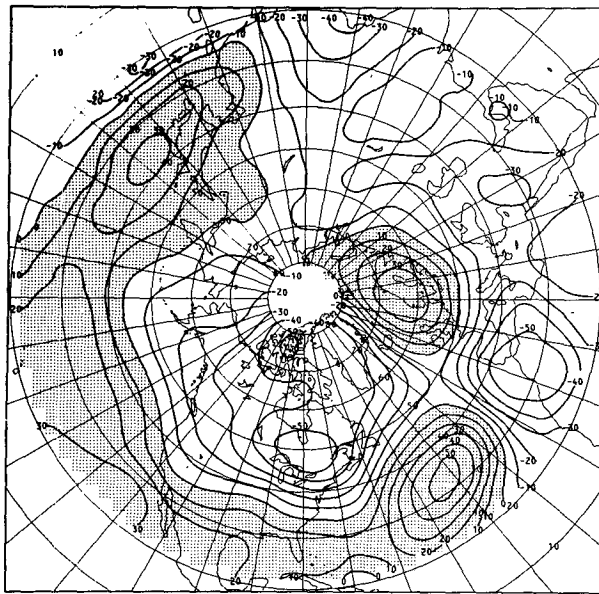


SON 700 MB ANOMALIES FOR LOW SOI YEARS, LAG=1

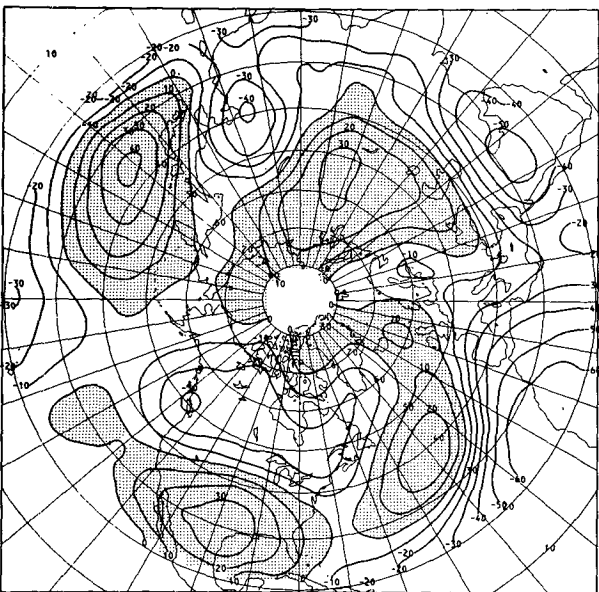


CONF. LIMIT OF SON COMPOSITE FOR LOW SOI YRS, LAG=1

FIG. 11. As in Fig. 10, associated with low-SOI values.



CORRELATION BETWEEN MAM SOI & MAM 700 MB HEIGHT



CORRELATION BETWEEN DJF SOI & MAM 700 MB HEIGHT

FIG. 12. Teleconnections for the spring season. Temporal lead by SOI's are indicated. The shaded areas are positive and the contour interval is 0.1.

contemporaneous teleconnection pattern fails to reach the 95% confidence limit. But, the other two patterns do exceed it with wide margins. When the SOI leads the height field by two seasons, the resulting teleconnections well exceed the 99% confidence limit.

d. Winter composites

To discern the contributions to the teleconnection pattern by the large positive and negative SOI as-

sociated height anomalies, three classes of composites were obtained. The SOI's were first normalized with the individual seasonal standard deviations and then divided into three classes with approximately equal numbers of cases for each high, medium and low category. Table 4 lists the class into which a SOI value of a given season falls. The composite associated with the medium range SOI's is not interesting. In this section, we shall present the major features of the high and low SOI associated composites, with the determining SOI values being placed zero to two seasons ahead of the winter height field.

The composites for high and low SOI are shown in Figs. 7 and 8, respectively. As expected, the strongest SO signal appears in the composite when the SOI precedes the height field by one or two seasons. Note particularly the low/high departures in the North Pacific, the high/low departures over western Canada, and the low/high departures over the eastern United States and western Atlantic area associated with the low/high SOI.

To evaluate the significance of the anomalies in the composites, confidence limits were also obtained and presented in figures. For a level of significance of 5% and 1%, respectively, a one-tailed Student's *t* distribution was applied to determine the values of anomaly that is significantly different from the long-term seasonal mean. Those departures with, respectively, 95 and 99% confidence were connected together to form a contour. The significant anomalies can thus be easily identified in Figs. 7 and 8.

Based on the information revealed by the confidence limits, distinct differences in features between the high and low SOI composites can be found. In the low SOI composites, while the deepening of the Aleutian low and the strengthening of the Pacific westerlies are clearly seen, the positive height anomalies over western Canada and the negative anomalies over the eastern United States do not reach the level of 95% significance. On the other hand, the high SOI composites exceed that level in all three regions. To put the difference of feature in perspective, it is noted that the low SOI phases are associated with warmer equatorial central Pacific sea-surface temperatures (Rasmusson and Carpenter, 1982; Horel and Wallace, 1981).

In a Northern Hemisphere surface pressure and temperature analysis, van Loon and Madden (1981) suggest that the SO was sometimes strong enough to influence the North Atlantic circulation and sometimes not, stressing on stability of the teleconnection patterns obtained for different periods of time. Our results, in addition, indicate a significant association with the North Atlantic Oscillation when the SOI's are high but lacking a clear association when the SOI's are low.

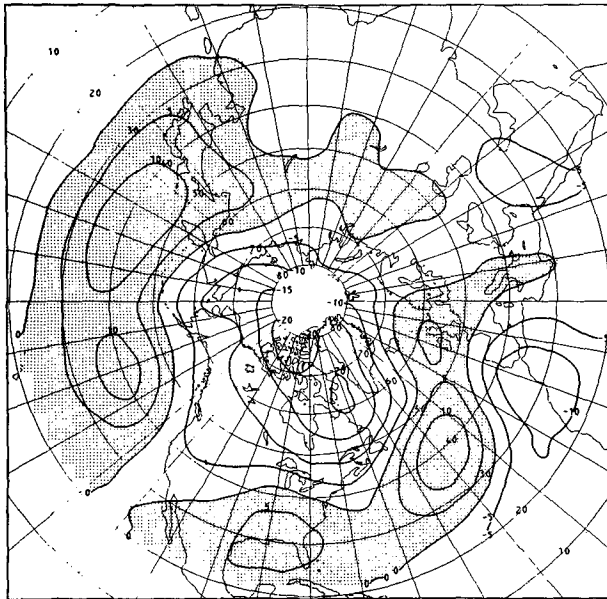
Also of interest in Figs. 7 and 8 is the shift from significant positive anomalies in the western sub-

tropical Pacific associated with the low SOI's to significant negative anomalies in South Asia associated with the high SOI's.

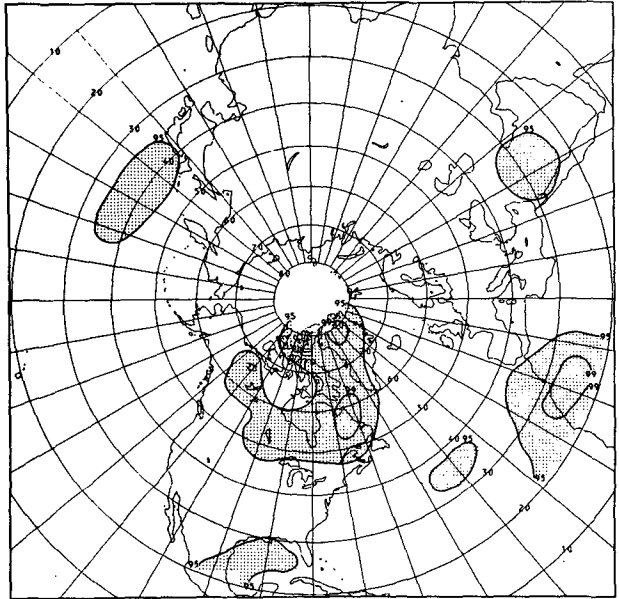
4. Autumn teleconnections and composites

The autumn results were obtained in the same manner as those for the winter season. High correlations are found in some areas for the contemporaneous one and when the SOI leads the height field

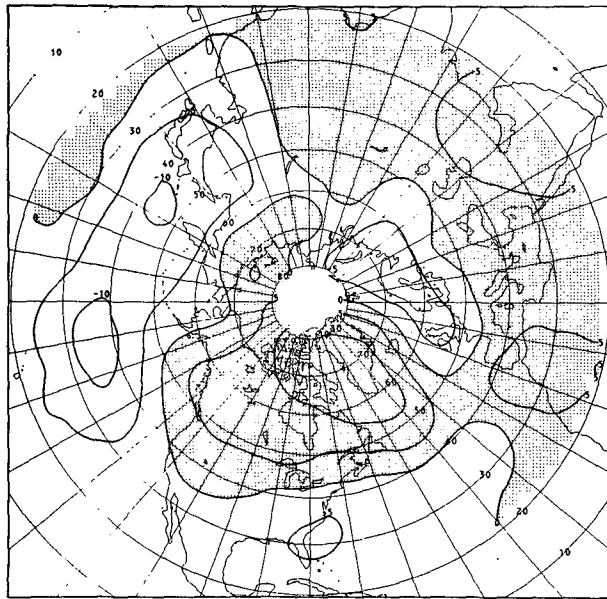
by about a season, as shown in Fig. 9. The correlation values of 5% significance level at five centers of higher correlation are listed in Table 2. They range from 0.36 to 0.39. The teleconnection pattern over the North Pacific-western Canada-eastern United States sector is similar to that of the winter season. Note, however, the significant change from the wintertime pattern in the north Atlantic. The positive correlation in the eastern United States extends



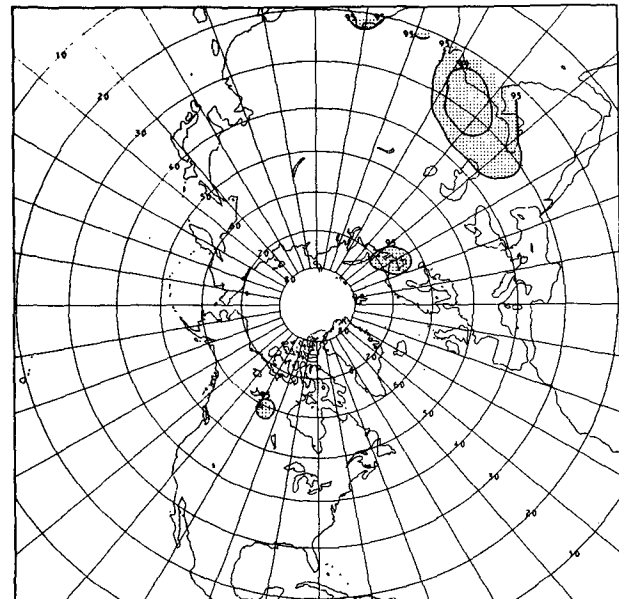
MAM 700 MB ANOMALIES FOR HGH SOI YEARS, LAG=0



CONF.LIMIT OF MAM COMPOSITE FOR HGH SOI YRS, LAG=0

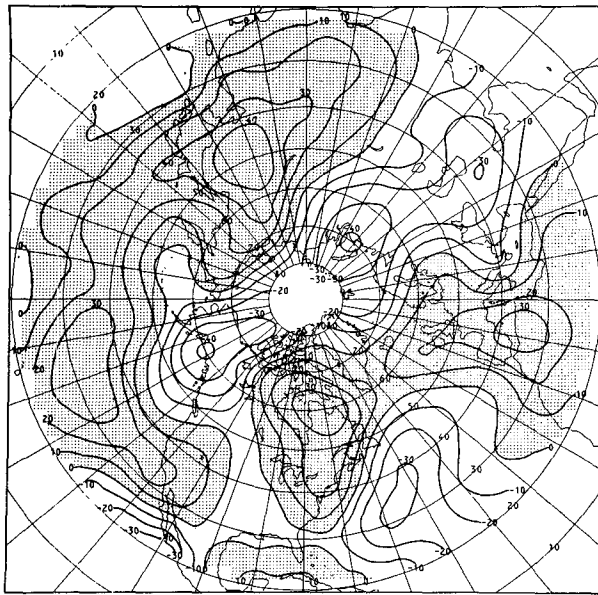


MAM 700 MB ANOMALIES FOR LOW SOI YEARS, LAG=0

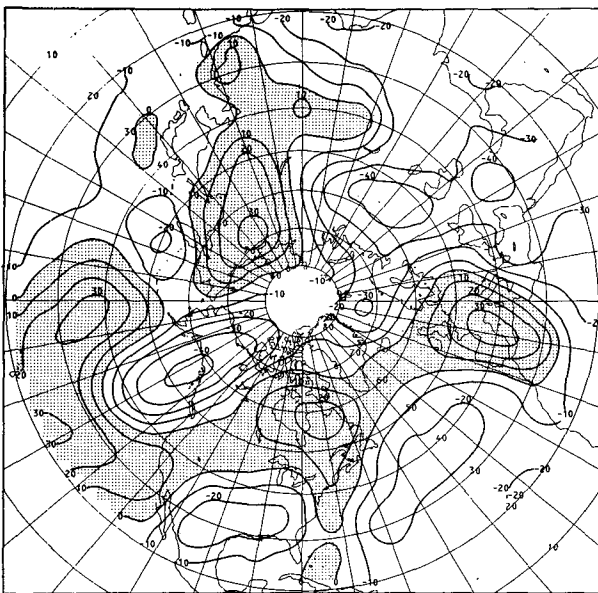


CONF.LIMIT OF MAM COMPOSITE FOR LOW SOI YRS, LAG=0

FIG. 13. Spring composites and confidence limits associated with high-SOI values (upper) and low-SOI values (lower). On the composites, the shaded areas are positive and the contour interval is 5 m.



CORRELATION BETWEEN JJA SOI & JJA 700 MB HEIGHT



CORRELATION BETWEEN MAM SOI & JJA 700 MB HEIGHT

FIG. 14. Teleconnections for the summer season. Temporal lead by SOI's are indicated. The shaded areas are positive and the contour interval is 0.1.

northward then southeastward to the coast of Portugal rather than extending eastward into the North Atlantic. The new teleconnection pattern in this United States–Canada–North Atlantic sector is well defined for the lag -1 correlation as well as the contemporaneous ones. The latter correlation pattern has 10.01% area exceeding critical values compared with 11.11% owing to chance occurrence with 5% significance level.

The composites of anomalies as well as the corresponding confidence limits for high and low SOI values are shown in Figs. 10 and 11, respectively. The most pronounced anomalies are associated with the strengthening/weakening of the Aleutian low. The positive anomaly in the eastern United States associated with the high SOI's appears to have a higher significance than the negative anomaly associated with the low SOI's. However, the positive/negative anomalies in the upper North Atlantic appear to be equally significant for both cases.

5. Spring teleconnections and composites

The teleconnection statistics for the spring season are shown in Fig. 12. The correlation values of 5% significance level at five centers of higher correlation are listed in Table 2. There is no significant correlation in the central north Pacific, but, around the north Atlantic, there is a strong negative–positive–negative pattern for the contemporaneous correlations, which has 11.92% area exceeding critical values compared with 12.38% due to chance occurrence with 5% significance level. The teleconnection weakens considerably for lag -1 cases. In the western North Pacific, however, the SO signals appear to be significant. The composites, shown in Fig. 13, indicate that the height anomalies in both sectors are significant, but for high SOI cases only.

6. Summer teleconnections and composites

The cross-correlations are much weaker in the summer than in the other three seasons. The teleconnection patterns and composites with zero lag are shown in Figs. 14 and 15, respectively. When the Monte Carlo technique was applied, the pattern failed to pass the significance test. The regions that might have some association with the SO are the Gulf of Alaska and northeastern China. In the latter region, both the high and low SOI associated anomalies are significant with 95% confidence. In the Gulf of Alaska, only high SOI associated anomalies may have some significance.

7. Summary and remarks

The variations in the Northern Hemisphere mid-troposphere circulation associated with the SO are investigated using mean monthly 700 mb height data for the period 1951–79. The lagged as well as contemporaneous correlations and composites of anomalies are presented for all four seasons.

Different teleconnection patterns are observed. The winter correlations are strongest and the summer the weakest. The winter positive–negative–positive teleconnection pattern over the North Pacific–western Canada–southeastern United States sector is similar to that shown by Bjerknes (1966, 1969), and,

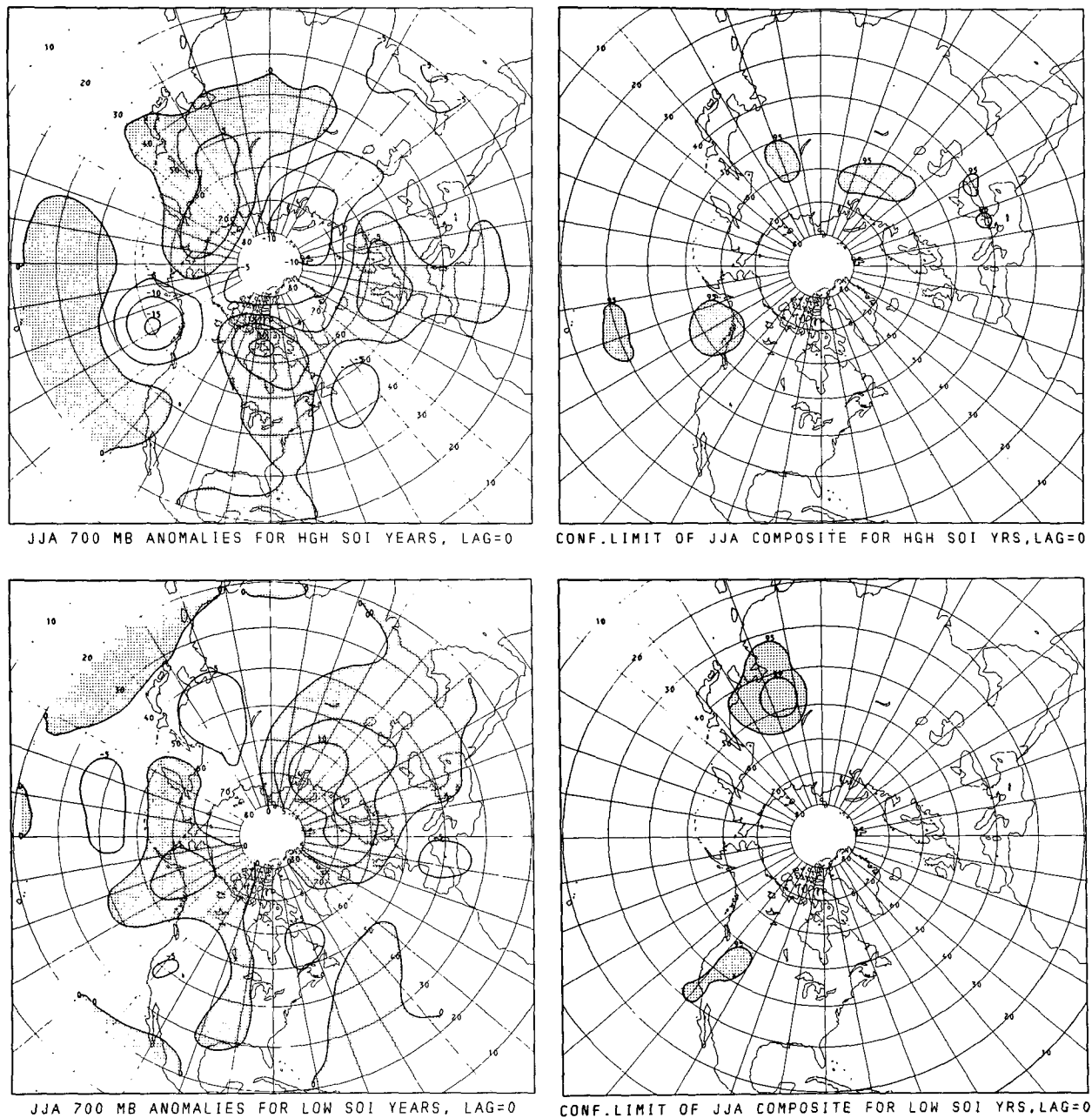
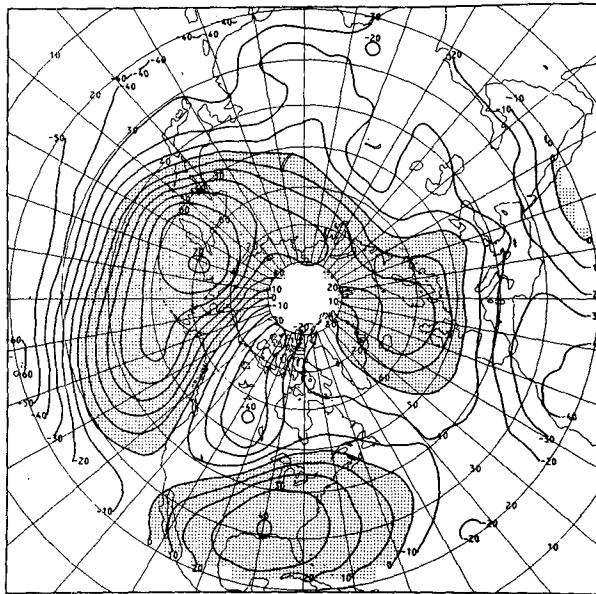


FIG. 15. Summer composites and confidence limits associated with high-SOI values (upper) and low-SOI values (lower). On the composites, the shaded areas are positive and the contour interval is 5 m.

most recently, Horel and Wallace (1981), van Loon and Madden (1981), van Loon and Rogers (1981) and Trenberth and Paolino (1981). Over the same sector, the autumn teleconnections have the same pattern, but they differ from the winter pattern over the North Atlantic sector. Centered around the North Atlantic another pattern is observed for the spring teleconnections. The correlation in summer is negligible.

Based on the theoretical studies of Opsteegh and

Van den Dool (1980), Webster (1981) and Hoskins and Karoly (1981), Horel and Wallace (1981) provide a plausible explanation of the physical process that links the SO to the middle latitudes. Responding to the forcing of the sea surface temperature (SST) and the rainfall in the equatorial central Pacific, the steady-state, linearized primitive equations on a sphere yield wave trains as well as vertical structures that bear qualitative resemblance to those SO teleconnection patterns observed in the North Pacific-



CORRELATION BETWEEN MAM SOI & DJF 700 MB HEIGHT

FIG. 16. Winter teleconnections with the SOI's consisting of the sum of mean spring sea-level pressures at Rapa and Easter Islands, with SOI's leading the height fields. The shaded areas are positive and the contour interval is 0.1.

western Canada-southeastern United States sector. The seasonal dependency that the numerical solutions indicate, i.e., the forced Rossby waves are present only for the winter half of the year and absent for the other half, is also in agreement with the observations.

The lead/lag relationship between the SO and its associated extratropical 700 mb height anomalies is also explored. The SOI, consisting of the difference in normalized mean monthly sea-level pressures (SLP) at Tahiti and Darwin, was used to define the SO in this study. Lead/lag relationships have also been investigated using the sum of mean monthly SLP at Rapa (28°S, 144°W) and Easter Island (27°S, 109°W) as an SOI. The strongest SO signal appears in the winter anomalies when the (Tahiti - Darwin) index precedes the height field by one to two seasons and when the (Rapa + Easter Island) index precedes by three seasons (Fig. 16). This is consistent with the finding of Chen (1982) that the SO signal in the latter index leads the former by one to two seasons. Both sea-level pressure indices, therefore, appear to be useful in the prognostic applications.

The investigation of Chen (1982) reveals that the SO is not a standing oscillation. Furthermore, Rasmusson and Carpenter (1982) report that there is a close tie between the SO and El Niño events. In general, an El Niño sets in during the northern winter with a rapidly rising SST on the west coast of South America. The anomaly reaches a maximum in about

April and persists for several months. In the meantime, the warmer SST spreads westward along the equator toward the dateline where it reaches a maximum in about July and persists through all of the next northern winter. The rainfall in the equatorial central Pacific also reaches maximum at this time (Horel and Wallace, 1981). The long-term average pressure of the overlying air varies in similar fashion to that of the SST. It is thus clear, while the forced Rossby waves magnify their effects during the winter, the precursor is there in the (Tahiti - Darwin) index two seasons and in the (Rapa - Easter Island) index, or SST index of the west coast of South America, three seasons ahead. The usefulness of this information in long-range forecasts is self-explanatory.

Finally, in order to discern the contributions to the teleconnection pattern by the large positive and negative SOI associated height anomalies, composites of the 700 mb height were obtained. An interesting feature of the winter composites is the tendency for more pronounced North America negative anomalies and North Atlantic positive anomalies associated with the high-SOI values, suggesting an association of the SO with one of two phases of the North Atlantic Oscillation. No such association is indicated by the low-SOI winter composites. For other seasons, the high-SOI composites also show more pronounced anomalies in various regions.

Acknowledgments. The author wishes to thank Drs. Eugene M. Rasmusson and Donald L. Gilman for their interest, encouragement and improvement in this work. The suggestions to include a discussion on the statistical significance of a spatial pattern from Dr. Robert E. Livezey is also gratefully acknowledged. The author also wishes to thank Mr. Michael C. Gaidurgis for drawing the figures and Ms. Gail S. Lucas for typing the manuscript. This is an Equatorial Pacific Ocean Climate Studies contribution, No. 15.

REFERENCES

- Berlage, H. P., 1957: Fluctuations of the general atmospheric circulation of more than one year, their nature and prognostic value. *Mededel. Verhandel Koninkl. Ned. Meteor. Inst.*, No. 69, 152 pp.
- , 1966: The Southern Oscillation and world weather. *Mededel. Verhandel. Koninkl. Ned. Meteor. Inst.*, No. 88, 152 pp.
- Bjerknes, J., 1966: A possible response to the atmospheric Hadley circulation to equatorial anomalies of ocean temperatures. *Tellus*, **18**, 820-829.
- , 1969: Atmospheric teleconnections from the equatorial Pacific. *Mon. Wea. Rev.*, **97**, 163-172.
- , 1972: Large-scale atmospheric response to the 1964-65 Pacific equatorial warming. *J. Phys. Oceanogr.*, **2**, 212-217.
- Chen, W. Y., 1982: Assessment of Southern Oscillation sea-level pressure indices. *Mon. Wea. Rev.*, **110**, 800-807.
- Davis, R. E., 1976: Predictability of sea-surface temperature and sea-level pressure anomalies over the North Pacific Ocean. *J. Phys. Oceanogr.*, **6**, 249-266.

- Dixon, W. J., and F. J. Massey, 1957: *Introduction to Statistical Analysis*. McGraw-Hill, 488 pp.
- Horel, J. D., and J. M. Wallace, 1981: Planetary scale atmospheric phenomena associated with the Southern Oscillation. *Mon. Wea. Rev.*, **109**, 813–829.
- Hoskins, J. B., and D. Karoly, 1981: The steady linear response of a spherical atmosphere to thermal and orographic forcing. *J. Atmos. Sci.*, **38**, 1179–1196.
- Julian, P. R., and R. M. Chervin, 1978: A study of the Southern Oscillation and Walker Circulation phenomena. *Mon. Wea. Rev.*, **106**, 1433–1451.
- Kidson, J. W., 1975: Tropical eigenvector analysis and the Southern Oscillation. *Mon. Wea. Rev.*, **103**, 187–196.
- Krueger, A. F., and J. Winston, 1974: A comparison of the flow over the tropics during two contrasting circulation regimes. *J. Atmos. Sci.*, **31**, 358–370.
- Namias, J., 1976: Some statistical and synoptic characteristics associated with El Niño. *J. Phys. Oceanogr.*, **6**, 130–138.
- Opsteegh, J. D., and H. M. Van den Dool, 1980: Seasonal differences in the stationary response of a linearized primitive equation model: Prospects for long range forecasting? *J. Atmos. Sci.*, **37**, 2169–2185.
- Quinn, W. H., 1974: Monitoring and predicting El Niño invasions. *J. Appl. Meteor.*, **13**, 825–830.
- Rasmusson, E., and T. Carpenter, 1982: Variations in tropical sea surface temperature and surface wind fields associated with the Southern Oscillation/El Niño. *Mon. Wea. Rev.*, **110**, 354–384.
- Trenberth, K. E., 1976: Spatial and temporal variations of the Southern Oscillation. *Quart. J. Roy. Meteor. Soc.*, **102**, 639–653.
- , and D. A. Paolino, Jr., 1981: Characteristic patterns of variability of sea level pressure in the Northern Hemisphere. *Mon. Wea. Rev.*, **109**, 1169–1189.
- Troup, A. J., 1965: The Southern Oscillation. *Quart. J. Roy. Meteor. Soc.*, **91**, 490–506.
- van Loon, H., and R. A. Madden, 1981: The Southern Oscillation. Part I: Global associations with pressure and temperature in northern winter. *Mon. Wea. Rev.*, **109**, 1150–1162.
- , and J. C. Rogers, 1981: The Southern Oscillation, Part II: Association with changes in the middle troposphere in the northern winter. *Mon. Wea. Rev.*, **109**, 1163–1168.
- Walker, G. T., and E. W. Bliss, 1932: World Weather V. *Mem. Roy. Meteor. Soc.*, **4**, 53–84.
- and ———, 1937: World Weather VI. *Mem. Roy. Meteor. Soc.*, **4**, 119–139.
- Webster, P. J., 1981: Mechanisms determining the atmospheric response to sea surface temperature anomalies. *J. Atmos. Sci.*, **38**, 554–571.
- Wright, P. B., 1977: The Southern Oscillation: Patterns and mechanisms of the teleconnections and the persistence. Rep. HIG 77-13, Hawaii Institute of Geophysics, University of Hawaii, 107 pp.
- , 1978: The Southern Oscillation. *Climate Variability—A Southern Perspective*, A. B. Pittock, L. N. Frakes and D. Jenness, Eds., Cambridge University Press, 180–185.
- , 1979: Hawaiian winter rainfall related to Pacific sea surface temperature. *Mon. Wea. Rev.*, **107**, 492–495.
- Wyrtki, J., 1973: Teleconnections in the equatorial Pacific Oceans. *Science*, **180**, 66–68.
- , 1975: El Niño—the dynamic response of the equatorial Pacific Ocean to atmospheric forcing. *J. Phys. Oceanogr.*, **5**, 572–584.